ROUND-TRIP TRAJECTORIES to MARS and VENUS *

Geza S. Gedeon **

Two types of round-trip trajectories are treated; "swing-around" trajectories, requiring no additional propulsion near the observation planet and "orbiting round-trip" trajectories, requiring propulsion to enter into a planetocentric orbit and to leave it after a specified waiting period. These problems are attacked by a new and very simple calculation procedure based on the "Lambertian Mechanics"[1] concept. The method presented is easily adaptable to an automatic digital computer, and thus it eliminates the tedious labor involved in constructing auxiliary charts and drawing envelopes to find optimum solutions.

Finally, in addition to the results in the usual form of graphs of total trip time versus characteristic velocity, the complete set of departure conditions is presented. These values can be used as good approximations to the initial conditions required by a precision orbit calculation routine.

INTRODUCTION

Exploration of outer space will undoubtedly start with inspection of the two nearest planets, Venus and Mars. The three steps probably required to accomplish this purpose are: (1) sending an instrumented package to these planets, (2) orbiting a crew around the planets, and (3) landing and returning a man from these planets. The second and third steps obviously involve round trips. However, it can be shown that "swing-around" trajectories offer many advantages over a one-way trajectory, even for the first phase. For example, the spacecraft would not be re-

quired to carry long-distance communication systems. Long read-out times on a home orbit or recovery of observations are permitted, and the penalties associated with the extra propulsion requirements at the planet are removed. For these reasons it was deemed advisable to undertake an analysis of round-trip trajectories only.

Swing-around trajectories were first proposed by Ehricke et al.[2] Battin[3] investigated a class of trajectories having velocities of departure restricted to values producing total trip times in the two-to-three-year range. Johnson and Smith[4] have made the very interesting discovery that trajectories of 1-to 1.5-years duration can be realized with velocity requirements which are feasible with present day technology. This last publication is, to the writer's knowledge, the only one dealing comprehensively with swing-around trajectories, presenting both swing-in and swing-out trajectories for different values of closest planetary approach. Unfortunately, as confirmed by private communication with the author of that paper, a programming error has resulted in certain errors in the results presented.

The second class of trajectories, the so-called orbiting round trips, involve a stay on the planet or on a planetary orbit, i. e., the space vehicle moves in heliocentric space with the same speed as the planet for a prescribed waiting time. To accomplish this feat, it is necessary to apply propulsion at arrival in the planetary vicinity and at take-off from the planet or planetary orbit. Unlike the swing-around trips in which total trip time and closest approach completely define the trajectory, an infinite number of orbiting round-trip trajectories are possible for a given total trip time and orbiting altitudes. This being the case, it is logical to search for optimum solutions. Moeckel[5] made the first step towards optimization by employing transfer trajectories which are tangent to the heliocentric orbits at departure. He found that nonsymmetric trajectories yield considerably lower trip times than symmetric ones for equal fuel requirements. Johnson and Smith[4] took the next logical step by removing the tangency requirement. They utilized a set of working charts and a

graphical optimization technique (envelope drawing) to obtain optimum orbiting round-trip trajectories to Mars. It is important to note that they realized that optimum round trips do not consist of two optimum one-way trajectories; rather, the optimization is utilized to determine the two segments into which the total trip should be divided. Johnson and Smith utilized a set of orbital equations developed by Moeckel (based on perihelion radii and velocities). Dugan[6] repeated the study of Martian round-trip trajectories using Vertregt's[7] method (based on eccentricity and semi-latus rectum) and extended it to cover Venutian[8] round trips. His method also utilized a set of working charts and graphical optimization.

In this paper, a new method of calculation based on the "Lambertian Mechanics"[1] is presented. The advantages of this method are twofold. First, the equations are continuous, i. e. , they provide a smooth transition between the routes called, by the earlier authors, direct, perihelion, aphelion, and indirect. Second, the equations are so simple that no intermediate working charts are required, and the optimization can be readily performed by an automatic digital computer.

Symbols

μ	GM = force field constant
a	semimajor axis
e	eccentricity
r	radius
q	$\dfrac{r}{2a}$ = modulus
c	chord
s	$\dfrac{r_o + r + c}{2}$ = semiperimeter
w	$\pm\sqrt{1 - c/s}$ = shape factor
z	$\dfrac{s}{2a} = \left(\dfrac{s}{r}\right) q$ = argument of universal time equation
V_h	$\sqrt{\dfrac{\mu_s}{r}}$ = heliocentric circular orbit velocity at radius r
V_p	$\sqrt{\dfrac{\mu_P}{r}}$ = planetocentric circular orbit velocity at radius r
K	$\dfrac{V}{V_h}$ or $\dfrac{V}{V_p}$ = heliocentric or planetocentric Kepler number
$K^{h.e.}$	hyperbolic excess Kepler number
ΔK	Kepler number increment
t	time, mean solar days
T	round-trip time, mean solar days
n	$\sqrt{\mu_S/r^3}$ = heliocentric angular velocity
θ	true anomaly
ϵ	transfer angle
α	Lambert's first angle
β	Lambert's second angle
ϕ	angle of elevation
γ	angle between chord and radius

σ	angle between hyperbolic excess velocity vector and the heliocentric velocity vector of the planet
κ	angular deflection at hyperbolic encounter
δ	angle measured from planet-sun line to planetary radius at departure from parking orbit, positive in direction of motion
A_n	$\dfrac{1.\,3.\,5.\ \ldots\ (2n-1)}{2.\,4.\,6.\ \ldots\ (2n)}$, $A_o = 1$ coefficients of the universal time equation
k	± 1 switching constant

Subscript

o	conditions at Earth
s	semiperimeter
S	Sun
E	Earth
h	heliocentric
p	planetary or planetocentric
w	waiting
1	outward leg
2	homeward leg
a	asymptote

ANALYSIS

Assumptions

The following assumptions are utilized in this analysis:

(1) The orbits of Earth, Mars, and Venus are circular and coplanar.

(2) The vehicle is attracted by only one inverse-square central force field at a time. No account is taken of transition from one sphere of influence to another in the vicinity of a planet, and the point at which the spacecraft enters or leaves the heliocentric force field is taken to be identical to the planet's position.

(3) The impulsive velocity-change concept is applied.

(4) Characteristic velocity rather than mass ratio is used as figure of merit.

Swing-Around Trajectories

A typical swing-in trajectory is shown in Fig 1. A trajectory cutting the planet sun line is designated a swing-out trajectory while one passing outside this line is designated a swing-in trajectory.

The analysis starts by assuming a heliocentric velocity vector at arrival to the vicinity of the target planet. The magnitude of the velocity is expressed by a unitless quantity, the Kepler number K_1. In Ref. 1, the source of many of the following equations, the Kepler number is defined as the actual velocity dividend by the local circular velocity. In this case, the latter corresponds to the heliocentric orbital velocity of the planet. The direction of the velocity vector is given by the angle of elevation ϕ_1.

Knowing the arrival velocity vector with magnitude and direction denoted by $\left[K_1, \phi_1 \right]$ and the planet's assumed circular velocity vector $\left[1, 0 \right]$, the hyperbolic excess velocity $K^{h.\,e.}$ can be calculated simply as the relative velocity with respect to the planet.
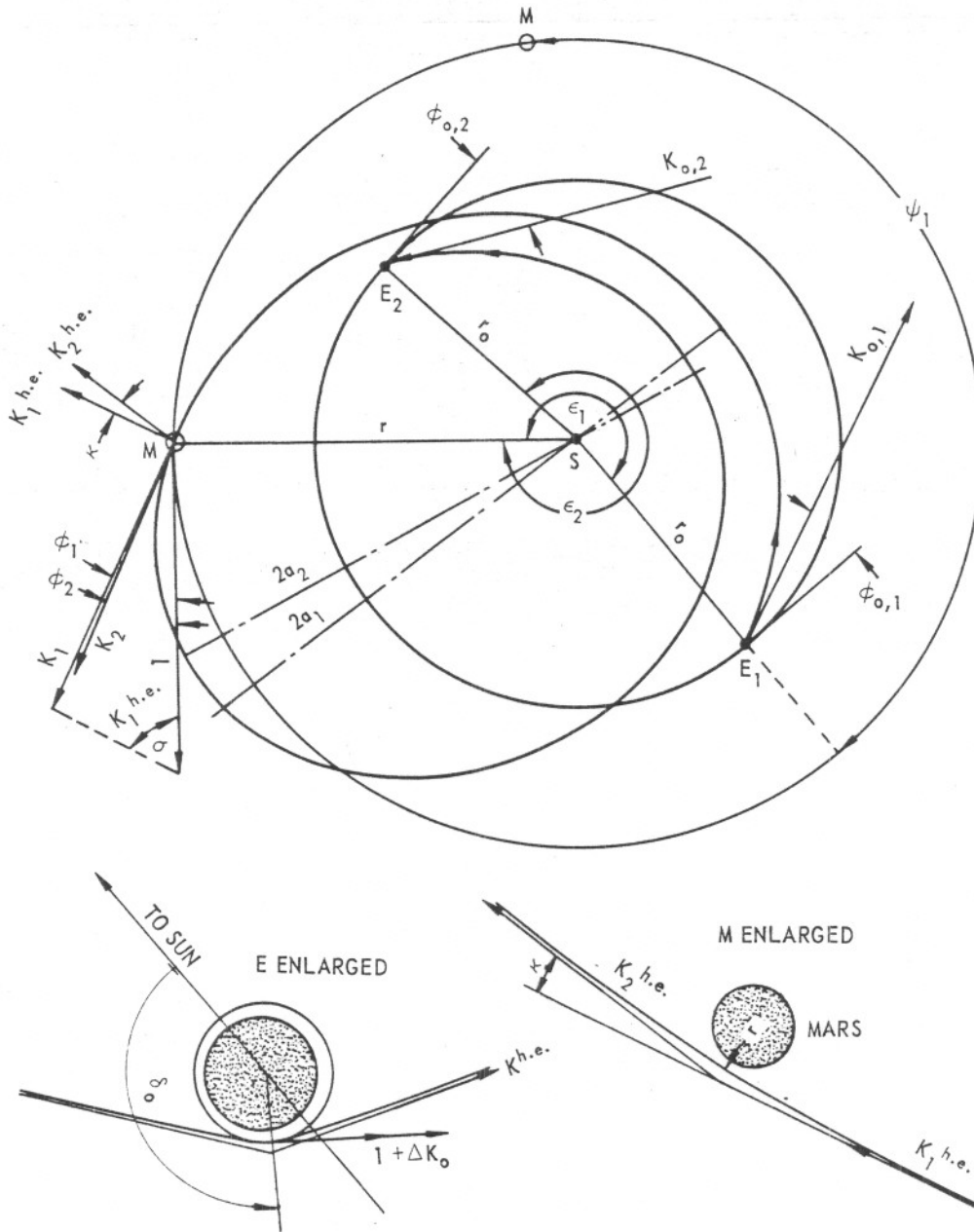
Fig. 1   A Swing-in Trajectory

$$K_1^{h.e.} = \sqrt{1 - 2K_1 \cos \phi_1 + K_1^2} \tag{1}$$

On the enlarged view of point M it can be seen that $K_1^{h.e.}$ is the approach velocity on the asymptote of a planetocentric hyperbola. The spacecraft departs along the other asymptote with hyperbolic excess velocity, $K_2^{h.e.}$, having the same magnitude as $K_1^{h.e.}$.

The gravitational attraction results in a deflection angle, , which is

$$\csc K/2 = \left[\frac{K^{h.e.}}{V_p/V_h} \right]^2 + 1, \quad 0 \leq \frac{K}{2} \leq \frac{\pi}{2} \tag{2}$$

The above relationship is derived in Appendix A.

In this equation, V_p is the planetocentric circular orbit velocity at closest approach and V_h is the heliocentric velocity of the planet. The angle σ included between $K_1^{h.e.}$ and the heliocentric velocity vector of the planet is obtained from

$$\sin \sigma = \frac{K_1}{K_1^{h.e.}} \sin \phi, \quad \left. \begin{matrix} 0 \leq |\sigma| \leq \frac{\pi}{2} \\ \frac{\pi}{2} \leq |\sigma| \leq \pi \end{matrix} \right\} \text{ if } K_1 \cos \phi_1 \left\{ \begin{matrix} < 1 \\ > 1 \end{matrix} \right. \tag{3}$$

$K_2^{h.e.}$ makes an angle $(\sigma \pm K)$ with the planets heliocentric velocity vector.

Now, the departure velocity vector can be calculated as the resultant of the heliocentric velocity of the planet and the hyperbolic excess velocity at departure by the relationships

$$K_2 = \sqrt{\left[1 - K_2^{h.e.} \cos (\sigma \pm K) \right]^2 + \left[K_2^{h.e.} \sin (\sigma \pm K) \right]^2} \tag{4}$$

and

$$\tan \phi_2 = \frac{K_2^{h.e.} \sin (\sigma \pm K)}{1 - K_2^{h.e.} \cos (\sigma \pm K)}, \quad -\frac{\pi}{2} \leq \phi_2 \leq \frac{\pi}{2} \tag{5}$$

Knowing the velocity vector at one end of the trajectory defines the or-bital segment. Thus, according to Ref. 1, the two moduli q, q_o are given by

$$q = 1 - \frac{1}{2} K^2, \quad q_o = \frac{q}{r/r_o} \qquad (6)$$

and the transfer angle ϵ by

$$\tan \epsilon/2 = \frac{1 - q/q_o}{- \tan \phi \pm \frac{q}{q_o} \sqrt{\frac{1-q_o}{1-q} \quad \frac{q_o}{q} \sec^2 \phi - 1}} \qquad 0 \leq \frac{\epsilon}{2} \leq \pi \qquad (7)$$

The $\pm$ sign in the above equation is due to the fact that conics are sym-metric around the line of apsides. In one case the trajectory contains one more apsis than in the other. Note that the above expression is based upon angle of elevation at the target planet, contrasted to the equation of Ref. 1, which was based on the initial angle of elevation. The difference between the two equations stems from the fact that the naught subscript is maintained, describing conditions at Earth. To use Eq. (7) for the second segment, the departure velocity vector is rotated through 180°, i.e., the sign of ϕ_2 is reversed. One thus has two orbital segments originating from the departure and arrival position of the Earth and meeting head-on at closest approach to the planet.

Next, according to Ref. 1, the transfer times t_1 and t_2 are calculated by first determining the chords c_1 and c_2 from

$$\frac{c}{r_o} = \sqrt{1 + (r/r_o)^2 - 2(r/r_o) \cos \epsilon} \qquad (8)$$

the semiperimeters s_1 and s_2 from

$$s/r_o = \frac{1 + r/r_o + c/r_o}{2} \qquad (9)$$

596

the shape factors w_1 and w_2 from

$$w = \pm \sqrt{1 - c/s} \qquad \begin{cases} + \text{ for } \epsilon < \pi \\ - \text{ for } \epsilon > \pi \end{cases}, \qquad (10)$$

and, finally, the transfer time from

$$n_s t = (1 - k) \frac{\pi}{(2z)^{3/2}} + k\sqrt{2} \sum_{n=0}^{\infty} A_n \frac{1 - kw^{2n+3}}{2n + 3} z^n \qquad * \qquad (11)$$

where

$$k = \pm 1, \quad n_s = \frac{n_E}{(s/r_o)^{3/2}}$$

n_E being the heliocentric angular velocity of Earth and

$$z = \frac{s}{2a} = \left(\frac{s}{r_o}\right) q_o \qquad (12)$$

In Eq. (11), the ambiguity is hidden in the expression k which is restrict-ed to +1 or -1. The plus sign applies when the empty focus falls outside the area enclosed by the segment and chord, the 'minus' sign when it falls inside. To determine the correct sign, the angle γ included be-tween the chord and the radius to the planet is computed by

$$\tan \gamma = \frac{\sin}{r/r_o - \cos \epsilon} \qquad \begin{cases} \text{if in } 3^{rd} \text{ or } 4^{th} \text{ quadrant} \\ \text{subtract } 2\pi \text{ from } \gamma \end{cases} \qquad (13)$$

and then compared with 2ϕ. The criterion used in Ref. 1 is adapted to the end conditions in the following manner,

$$\text{if} \quad \begin{cases} \gamma > (-2\phi) \\ \gamma < (-2\phi) \end{cases} \qquad \begin{cases} k = +1 \\ k = -1 \end{cases}$$

Since Eq. (7) is double valued and there are two segments, four individ-ual trip time values are calculated: t_1', t_1'', t_2', t_2'', the first two

* See Ref. 1 about the convergence of above series.

597

corresponding to the first leg and the last two to the last leg. If any of the four combinations satisfy the requirement that

$$(t_1 + t_2) \, n_E = (\epsilon_1 + \epsilon_2)$$

where n_E is the angular velocity of Earth in the same units as t_1 then departing from Earth at the correct date, the returning space vehicle will intercept Earth at the end of the trip.

If none of the combinations satisfies Eq. (14), then one of the initial assumptions must be changed. K_1 can be kept fixed and $\varnothing_1$ varied between arbitrary limits (high $\varnothing_1$ means high propulsion requirement) or $\varnothing_1$ fixed and K_1 varied. Both solutions are double valued in certain regions. Thus, care must be exerted to find both solutions.

If a solution to Eq. (14) is found, the constellation angle can be calculated from

$$\psi_1 \quad = \epsilon_1 - n_p \, t_1 \tag{15}$$

where $n_p = n_E/(r/r_o)^{3/2}$ is the angular velocity of the planet. It is supposed that departure will be made from a geocentric parking orbit in the plane of the ecliptic. The amount of velocity increment necessary for departure can be calculated in the following manner.

First, the departure Kepler number is given by

$$K_o \quad = \sqrt{2(1 - q_o)} \tag{16}$$

and the angle of elevation at departure by

$$\cos \phi_o \quad = \sqrt{\frac{(1 - q) \, q}{(1 - q_o) \, q_o}} \; \cdot \; \cos \phi \tag{17}$$

Note that the sign of ϕ_o is undetermined; it agrees with ϕ if the number of apsides in the trajectory is even (0 or 2), and differs from ϕ if this number is odd. The number of apsides may be determined from the nature of the problem. This ambiguity can be avoided by using Eq. (27).

Next, the hyperbolic excess velocity $K_o^{h.e.}$ is obtained by Eq. (1) and then the heliocentric Kepler number increment ΔK_o from

$$\Delta K_o = \sqrt{(K_o^{h.e.})^2 + 2\left[\frac{V_p}{V_h}\right]_E^2} - \left[\frac{V_p}{V_h}\right]_E \tag{18}$$

where $(V_p)_E$ is the geocentric circular velocity on the parking orbit and $(V_h)_E$ is the heliocentric velocity of Earth. Thus, ΔK_o is normalized with respect to the Earth's heliocentric velocity (18.5 mi/sec or 29.8 km/sec).

The point of application of this impulse is assumed to be the vertex of the geocentric hyperbola of departure. To find the angle δ_o between the axis of this hyperbola and the Earth - Sun line, Eqs. (2) and (3) are employed again, using departure data (naught subscript). The angle δ_o is given by

$$\delta_o = (\sigma_o - K_o/2) \tag{19}$$

The calculation of ΔK_o and δ_o can be repeated for the return point, and a characteristic velocity can be obtained by adding together the two impulses.

Orbiting Round Trip Trajectories

Figure 2 shows an orbiting round-trip trajectory. During the given waiting time t_w, the spacecraft moves through the angle ϵ_w with the angular velocity of the planet in heliocentric space where

$$\epsilon_w = n_p t_w \tag{20}$$

The total angle ϵ swept out by the Earth during the round trip is defined by the given total trip time t

$$\epsilon = \epsilon_1 + \epsilon_w + \epsilon_2 = n_E t \tag{21}$$

This last equation serves to define only the sum of the transfer angles ϵ_1 and ϵ_2, rather than the two angles individually. It is part of the opti-
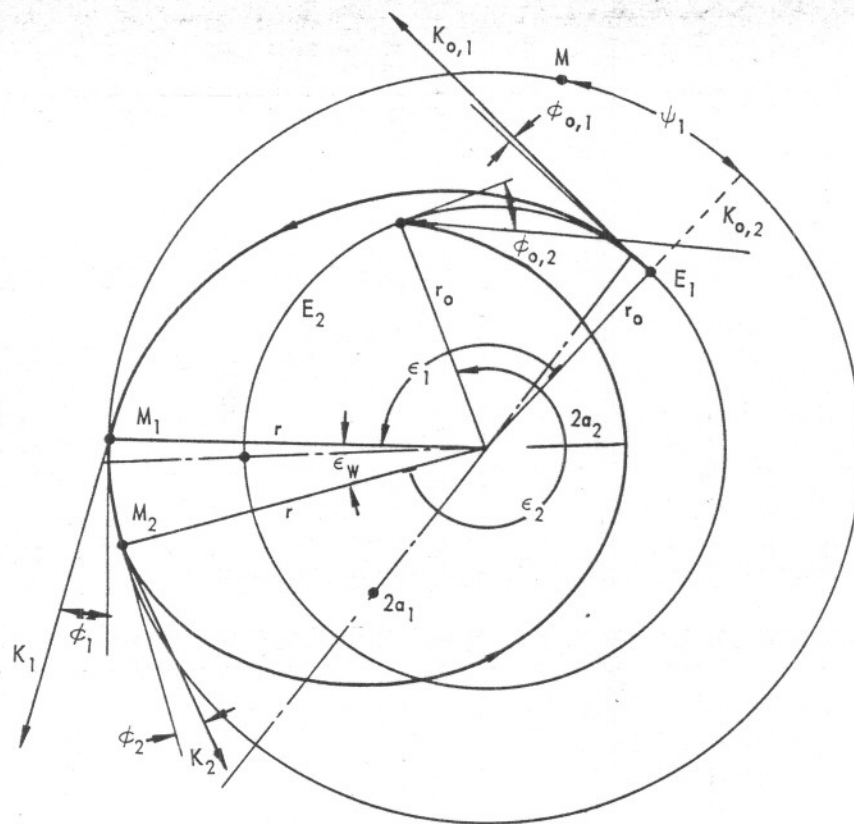
Fig. 2   An Orbiting Round Trip Trajectory

mization procedure to find each of the angles.   Thus the calculation be-
gins by assuming an ϵ_1 and a trajectory parameter of the first segment.
This fixes the transfer time, and an optimization subroutine varies ϵ_1
and the trajectory parameter until minimum characteristic velocity is
found.

The trajectory parameter selected can be either the modulus q or the
argument z defined in Ref. 1.   These quantities are interrelated by

$$z = \left(\frac{s}{r} \right) q \qquad (22)$$

where (s/r) is a constant if ϵ is fixed.   The choice of z is preferred
since it has a fixed upper limit = + 1, which is a convenience in auto-
matic machine calculations.

The calculation starts by computing the chords c_1 and c_2 by Eq. (8), the semiperimeters s_1 and s_2 by Eq. (9), and finally the shape factors w_1 and w_2 by Eq. (10).

The trip time t_1 can be calculated by Eq. (11). However, t_2 is defined by the relation

$$t_1 + t_w + t_2 = t \tag{23}$$

and therefore Eq. (11) should be used to calculate z_2. This appears to be a very cumbersome procedure. At the outset, it was hoped that a good approximation to the inverse of Eq. (11) could be found. Unfortunately this has not yet been realized. Therefore, a trial and error procedure has been used in programming this problem. For trial and error solution, Lambert's Equation in the form illustrated below was used in place of Eq. (11).

$$n_E t = \frac{(\alpha - \sin\alpha) - (\beta - \sin\beta)}{\left(\dfrac{2z}{s/r_o}\right)^{3/2}} \tag{24}$$

where

$$\alpha = (1-k)\,\pi + 2k\sin^{-1}\sqrt{z} \tag{25}$$

and

$$\beta = \pm \sin^{-1} w\sqrt{z} \qquad \begin{cases} + \text{ for } \epsilon < \pi \\ - \text{ for } \epsilon > \pi \end{cases} \tag{26}$$

Equations (24) through (26), along with Eq. (23), were used to solve directly for t_1 and by trial and error for z_2. The constant k_1 [k associated with the first leg] was an input, $k_1 = +1$ producing fast elliptic outward segments, and $k = -1$ allowing slow trajectories. The second constant k_2 [k associated with the second leg] was selected by the program. If no root has been found with $k_2 = +1$ then the machine switched automatically to $k_2 = -1$ to find z_2. No provision was made for parabolic or hyperbolic orbits since, in the total trip time range inves-

tigated, elliptic segment solutions were possible with considerable smaller fuel requirements.

As soon as z_2 was found, it was converted into the modulus q_2 by dividing by s/r. Then the Kepler numbers at the four endpoints of the two segments were calculated by Eq. (16) and the angles of elevation by the following equations

$$\tan \phi_o = \frac{1-q_o}{\tan \epsilon/2} \quad -k \quad \frac{\sqrt{(1-q_o)(q_o/q) - q_o \cos^2 \epsilon/2}}{\sin \epsilon/2} \tag{27}$$

and

$$\tan \phi = - \frac{1-q}{\tan \epsilon/2} + k \frac{\sqrt{(1-q)(q/q_o) - q(1-q\cos^2 \epsilon/2)}}{\sin \epsilon/2} \tag{28}$$

Note that the constant k must have the same value in these equations as used in Eq. (25).

Knowing the velocity vectors at the four endpoints (again both segments originate from the Earth and end at the planet at the arrival and departure position in heliocentric space), the hyperbolic excess velocities can be found by Eq. (1) and the Kepler number changes by Eq. (18).

Finally, the characteristic velocity (normalized to ecliptic speed) is

$$V_{CH}/(V_h)_E = \Delta K_{o, 1} + \frac{\Delta K_1 + \Delta K_2}{\sqrt{(r/r_o)}} + \Delta K_{o, 2} \tag{29}$$

To find minimum characteristic velocity, ϵ_1 and z_1 are changed by a subroutine utilizing a "gradient or steepest descent" method of optimization. When the minimum characteristic velocity is found, the departure conditions are calculated by the same procedure as in the case of swing-around trajectories, i.e., the configuration angle is obtained by Eq. (15), and the velocity increments for departures from an Earth orbit and from a planetary orbit by Eqs. (3) and (18).

RESULTS AND DISCUSSIONS

Solutions for Swing-Around Trajectories

Figures 3 and 4 illustrate velocity vectors (K, ϕ) at planetary encounter which produce round-trip trajectories originating and terminating at Earth under the assumption that the closest approach to the (center of the) planet is 1.1 planetary radius. Figures 5 and 6 illustrate several cases of particular interest.

Before attempting to explain the above solutions it is advisable to discuss the characteristics of those unperturbed trajectories which emanate from and return to Earth. One solution is obvious; all orbits having a semimajor axis identical to that of the Earth's heliocentric orbit (1 au) will intercept Earth a year later. Thus, the modulus of such an orbit at planetary encounter is one-half the mean radius of the planetary orbit expressed in au's. Then, Eq. (16) yields a heliocentric Kepler number at Mars of 0.6909 for all unperturbed one-year orbits. These orbits are represented by the vertical dotted line on Fig. 3. In the following sketches of unperturbed Martian orbits (Fig. 5), empty circles correspond to possible locations of massless planets. The filled circles correspond to planetary locations for which a perturbative analysis was carried out. The number 2 represents launch points for one-year orbits. The numbers 3 and 4 represent planetary locations at encounter. Number 5 designates an extra crossing of the Earth's orbit, and 6 the arrival position. For example, sketch (A) illustrates an orbit departing from Earth at point 2, passing by a massless Mars located at point 3/4, and returning to Earth at point 6 which is exactly coincident with the departure point.

However, one-year orbits do not constitute the only family of unperturbed orbits which intercept Earth at return. Martian orbits which overlap at perihelion can also be constrained to return to Earth by proper choice of the semimajor axis. The term 'overlapping' designates double

603
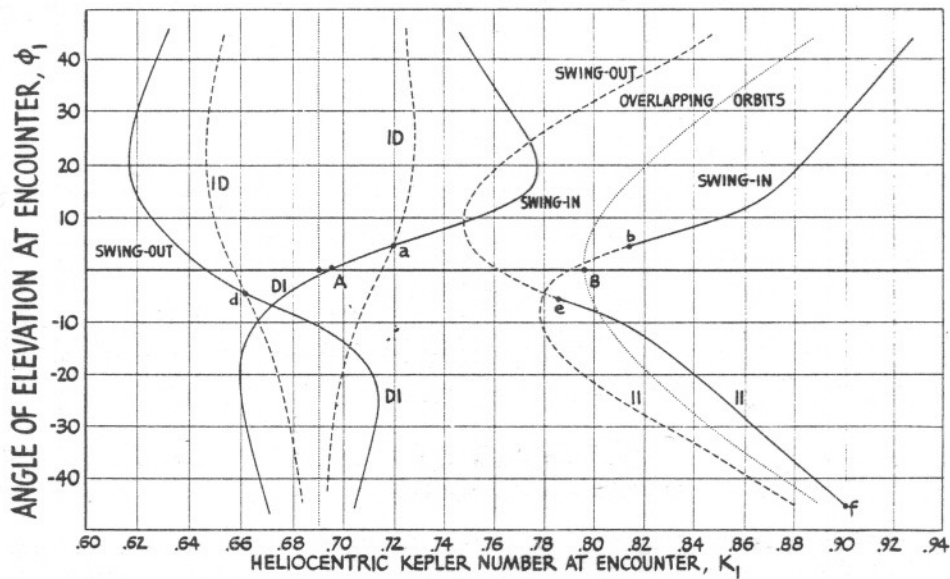
Fig. 3   Solutions to Swing-Around-Mars Trajectories.   Closest approach
1.1 M. R.

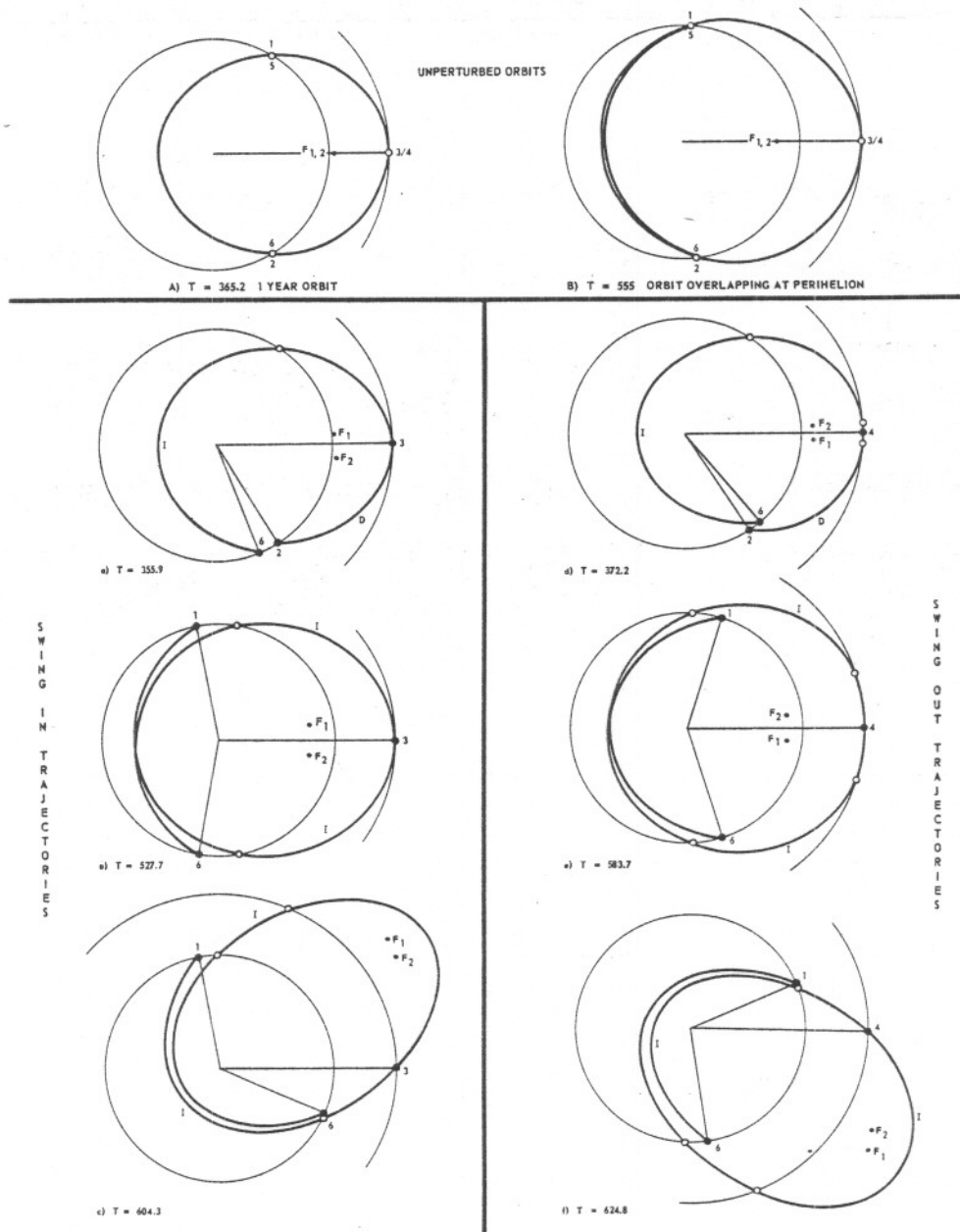Fig. 4   Swing-Around-Mars Trajectories

UNPERTURBED ORBITS

A) T = 365.2 1 YEAR ORBIT

B) T = 555 ORBIT OVERLAPPING AT PERIHELION

a) T = 355.9

d) T = 372.2

SWING IN TRAJECTORIES

SWING OUT TRAJECTORIES

b) T = 527.7

e) T = 583.7

c) T = 604.3

f) T = 624.8
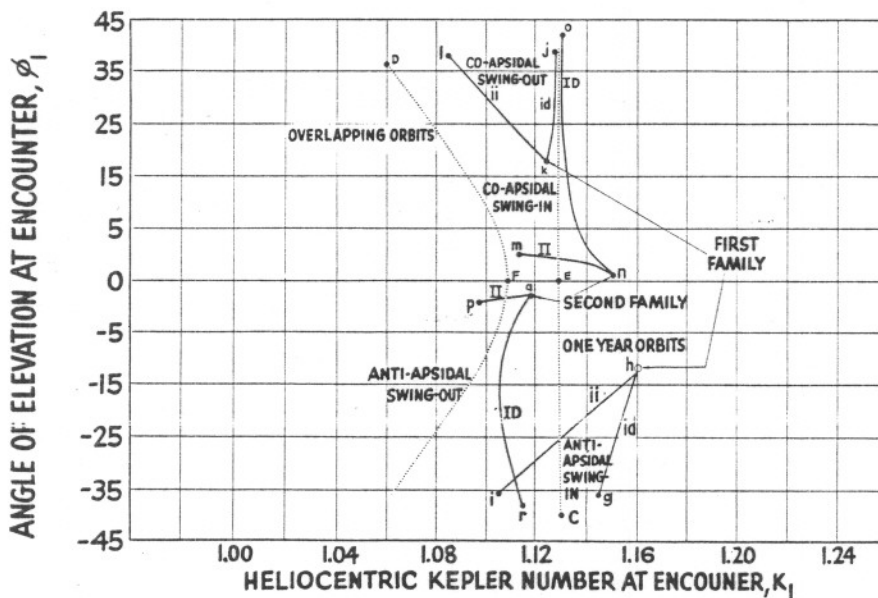
Fig. 5   Solutions to Swing-Around-Venus Trajectories. Closest approach
1. 1 V. R. First Family: lower case letters, Second Family:
capital letters (used for route designations)

C) T = 365.2 1 YEAR ORBIT

D) T = 437.7 ORBIT OVERLAPPING AT APHELION

SWING IN TRAJECTORIES

SWING OUT TRAJECTORIES

g) T = 393.2

h) T = 489.5

i) T = 452.7

j) T = 364.9

k) T = 387.3

l) T = 416.1

(a)
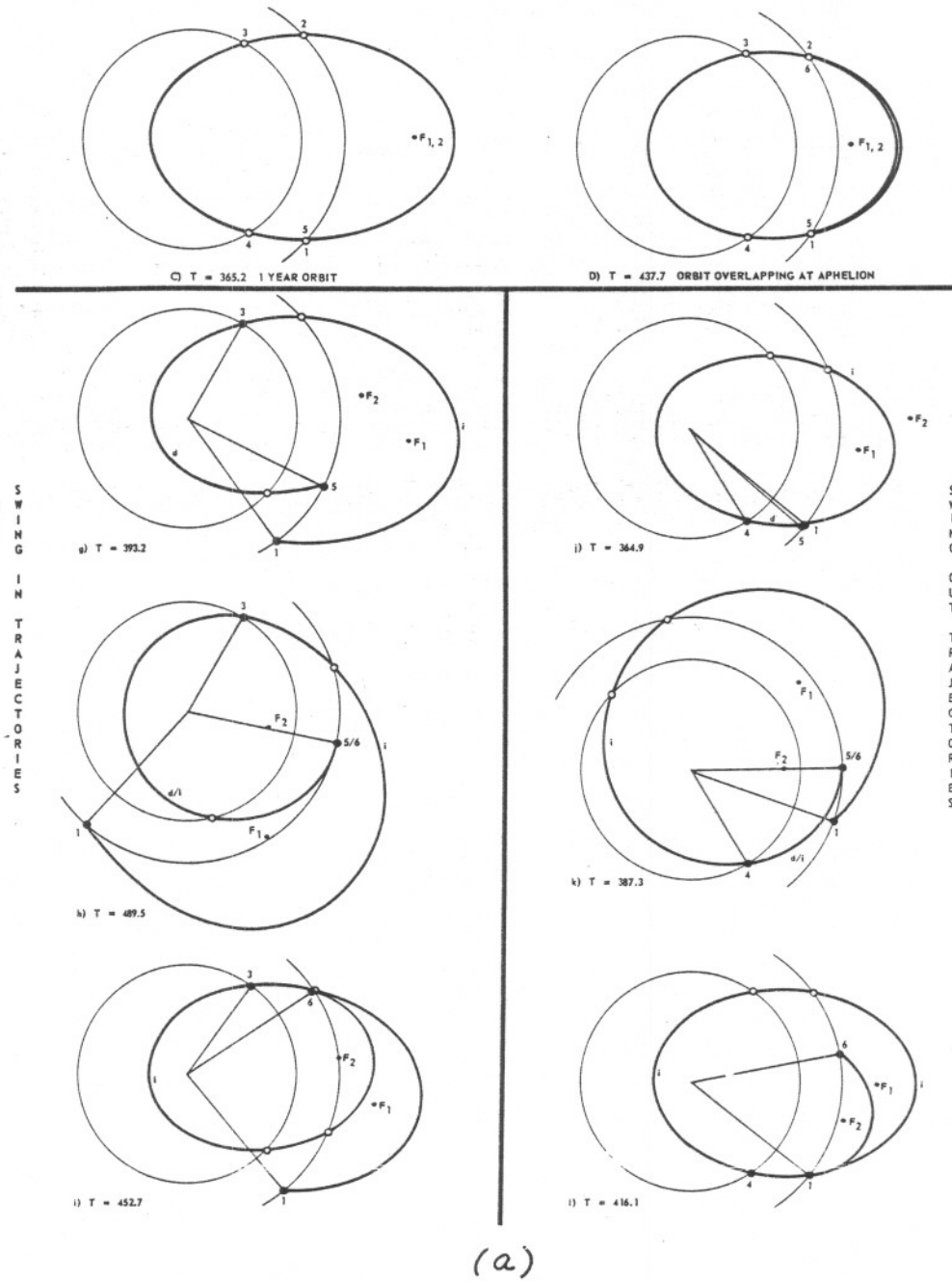
Fig. 6   Swing-Around-Venus Trajectories.   a) First Family b) Second
Family

606

UNPERTURBED ORBITS
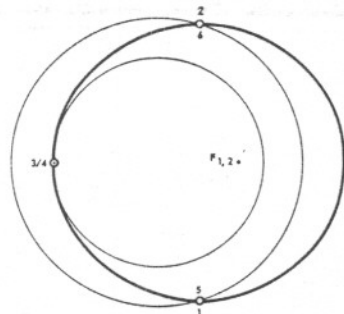
E) T = 365.2   1 YEAR ORBIT
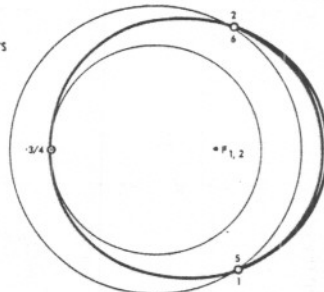
F) T = 488.2   ORBIT OVERLAPPING AT APHELION
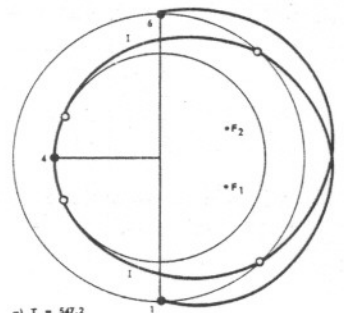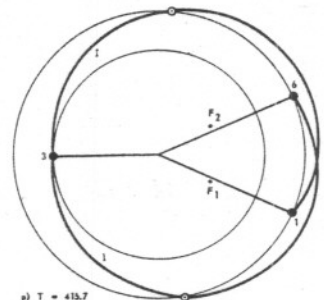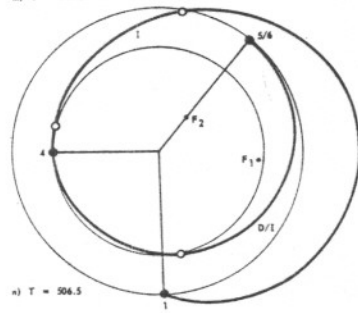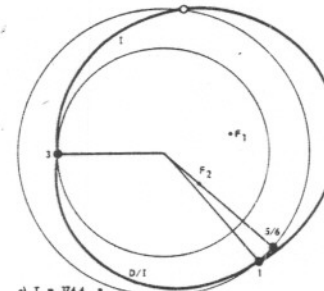
SWING OUT TRAJECTORIES

SWING IN TRAJECTORIES

SWING OUT TRAJECTORIES

o) T = 547.2

p) T = 415.7

n) T = 506.5

s) T = 374.4

o) T = 366.0

r) T = 336.6

(b)

Second

Fig. 6b

607
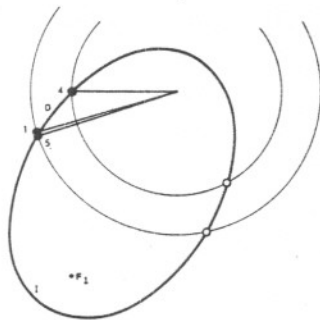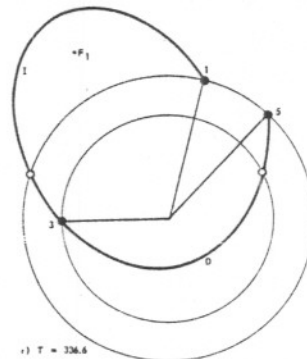
passes through perihelion for Martian orbits. The dotted curve on Fig. 3 illustrates such a family, and sketch (B) shows a particular trajectory of longer than one-year duration. It should be noted that for overlapping orbits, departure occurs at point 1.

Should the space vehicle pass outside the planet-sun line, the one year orbit (A) is perturbed into a swing-in trajectory, sketch (A). Similarly, if the vehicle cuts the planet-sun line, a swing-out trajectory results (sketch D). The full line curves on Fig. 3 passing through points a and d were obtained from analysis of perturbed one-year nominal orbits having higher eccentricities than (A). The corresponding dashed line curves represent mirror image trajectories, i.e., trajectories originating at 6 and terminating at 2. Such orbits can be envisioned as those obtained by reversing both vehicle and planetary motions. Hence, they will be designated clockwise trajectories.

Perturbing the overlapping orbit (B), produces trajectories (c) and (e). Likewise, increasing the eccentricity of the original orbit results in curves passing through points c and e in Fig. 3. Although both sets of curves were not drawn beyond $\phi = \pm 45°$, solutions do exist beyond these values.

Each set of the trajectory is distinguished as between those which cross and do not cross the Earth's orbit; designated indirect and direct, respectively. It should be noted that these same adjectives have been used by other authors in a more restricted sense. Thus, the perturbed one-year orbits are considered direct-indirect, whereas the perturbed overlapping orbits are indirect-indirect.

Martian trajectories passing 2 and 5 planetary radii from the center of the planet were also investigated. Solutions similar to those illustrated in Fig. 3 were obtained. However, since the perturbation from a two-body orbit is smaller, deviations from the dotted curves are less pronounced.

on Fig. 3

ctory of

apping

e year

milarly,

sults

a and

bits

d line

origi-

as those

e, they

and (e).

lts in

sets of

ond these

ch cross

ct, re-

been used

bed one-

bed over-

enter of

lustrated

a two-

ss pro-

Figure 4 illustrates the much more complicated swing-around Venus trajectories. The vertical dotted line corresponds to one-year orbits in a manner wholly analogous to the one-year Martian orbits illustrated in Fig. 3. As in the case of Martian orbits, empty circles in Fig. 6 correspond to possible locations of massless planets, and filled circles to planetary locations obtained from perturbative analysis. Sketches (C) and (E) represent minimum eccentricity (tangent to Venus' heliocentric orbit at fly-by), unperturbed one-year orbits. Sketches (D) and (F) illustrate minimum eccentricity overlapping orbits. For Venusian trajectories the term "overlapping" designates double passes through aphelion. For these trajectories, departure always occurs at point 1, extra-Earth orbital crossing at 2, planetary encounter at 3 or 4 and arrival at either 5 or 6. Should planetary encounter occur when the Earth and the planet at encounter are on the same side of the line of apsides of the first orbital segment, the perturbation is called co-apsidal and the number 4 is used. In the other case, the perturbation is called anti-apsidal, and the number 3 is used. The definitions of co-apsidal and anti-apsidal perturbations, as based on departure and encounter positions, hold true if vehicle and planetary motions are reversed, i. e., if departure occurs at 6 and arrival at 1 or 2. Unperturbed overlapping orbits of longer than one-year duration are represented by the dotted curve on Fig. 4. It should be noted that the vertex of this curve is much closer to the straight vertical line than in the Martian case.

Unlike Martian trajectories whose ϕ vs. K graphs were found to be continuous, discontinuous solutions were found for all perturbed Venusian trajectories (Fig. 4). These discontinuities were found to occur around small angles of elevation splitting the curves into two parts corresponding to co-apsidal and anti-apsidal perturbations. The upper and lower halves of Fig. 4 correspond respectively to co-apsidal and anti-apsidal perturbations for counterclockwise trajectories as illustrated on Fig. 6. The analysis of clockwise trajectories is omitted on Fig. 4 because of

the obviously greater complexity of Venusian as compared with Martian trajectories. Considering first the anti-apsidal case, the curves $\overset{\frown}{gh}$ and $\overset{\frown}{qr}$ can be regarded respectively as swing-in and swing-out perturbations of one-year orbits. Similarly, $\overset{\frown}{ih}$ and $\overset{\frown}{pq}$ may be regarded as representations of perturbed overlapping orbits. In the case of co-apsidal perturbations, $\overset{\frown}{jk}$ and $\overset{\frown}{on}$ were obtained from perturbations of one-year orbits, and $\overset{\frown}{lk}$ and $\overset{\frown}{mn}$ from perturbations of the overlapping orbit. It should be noted that k, n, q and h, representing tangential Earth arrival, are common points for pairs of curves. Such points do not exist if the perburbation is small, i.e., they do not appear for a closest approach of 5 Venusian radii.

Examination of Fig. 4 and the subsequent charts reveals a similarity in appearance between co-apsidal swing-out and anti-apsidal swing-in trajectories. For this reason, both types of trajectories will be designated as the First Family of swing-around Venus trajectories. Similarly coapsidal swing-in and anti-apsidal swing-out trajectories are grouped together as the Second Family. Figure 6a presents the First Family of swing-around Venus trajectories. Sketch (C) illustrates an unperturbed highly eccentric one-year orbit with (g) and (j) representing trajectories obtained by anti-apsidal swing-in and co-apsidal swing-out, respectively. Highly eccentric overlapping orbits are perturbed into trajectories (i) and (l). Similarly, (h) and (k) are obtained from less eccentric one-year orbits.

Figure 6b presents the Second Family of swing-around-Venus trajectories. The symmetric trajectories (m) and (p) are obtained by perturbations of minimum eccentricity unperturbed orbits (E) and (F), respectively. Trajectories (n) and (q) represent cases when arrival is tangential to the Earth's orbit. Finally, (o) and (r) illustrate highly perturbed one-year nominal orbits.
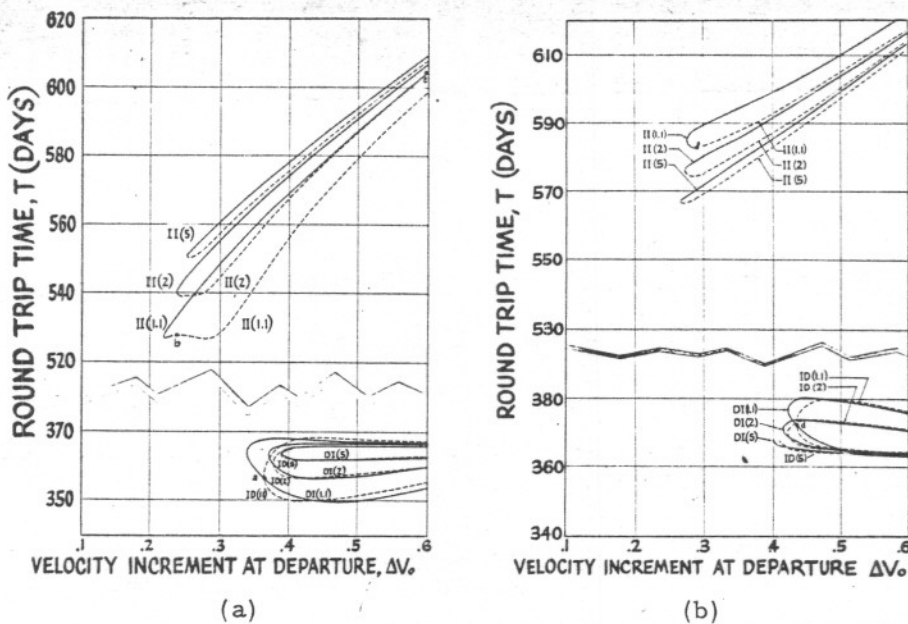
F

Fig. 7   Round Trip Time vs. Velocity Increment (normalized with the heliocentric velocity of Earth) for Swing-Around-Mars Trajectories. Parking Orbit 1.1 E. R. Closest approach 1.1, 2, 5 M. R. a) Swing-in b) Swing-out
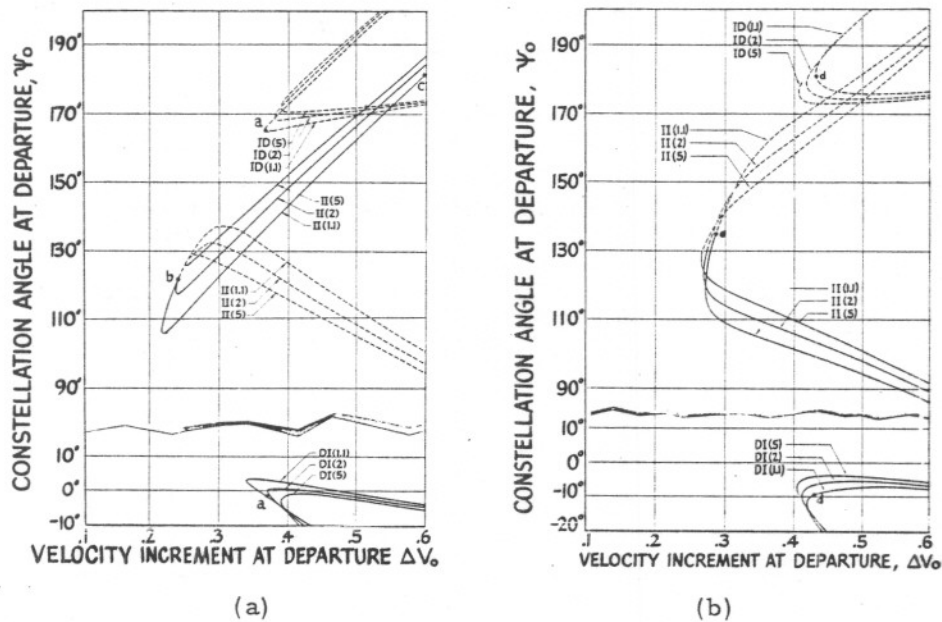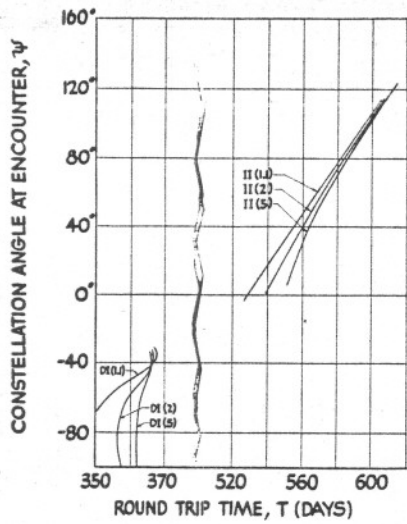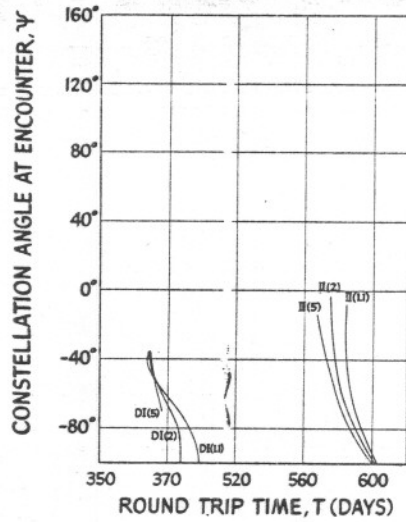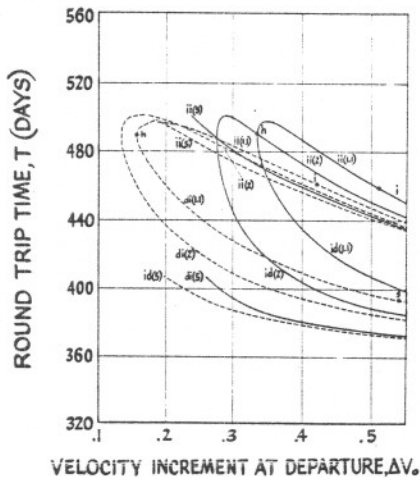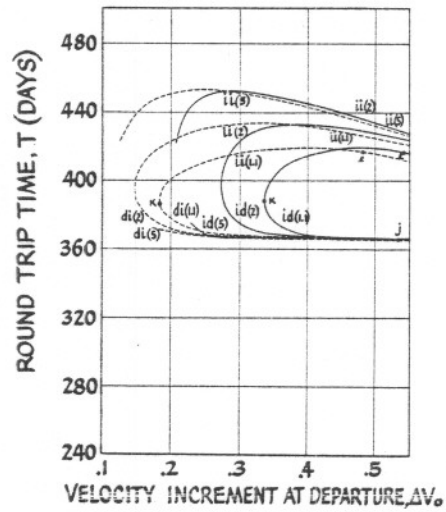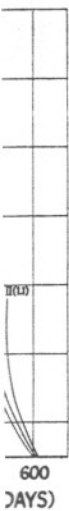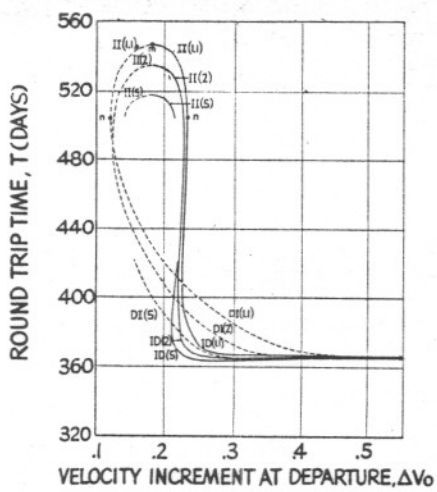

Fig. 8   Departure Constellation Angle vs. Velocity Increment (normalized with the heliocentric velocity of Earth) for Swing-Around-Mars Trajectories. Parking Orbit 1.1 E. R. Closest Approach 1.1, 2, 5 M. R. a) Swing-in b) Swing-out

611

Fig. 9 Encounter Constellation Angle vs. Total Trip Time for Swing-
Around-Mars Trajectories. Parking Orbit 1. 1 E. R. Closest
Approach 1. 1, 2, 5 M. R. a) Swing-in b) Swing-out

Fig. 10 Total Trip Time vs. Velocity Increment (normalized with the
heliocentric velocity of Earth) for Swing-Around-Venus Trajec-
tories. Parking Orbit 1. 1 E. R. Closest Approach 1. 1, 2, 5
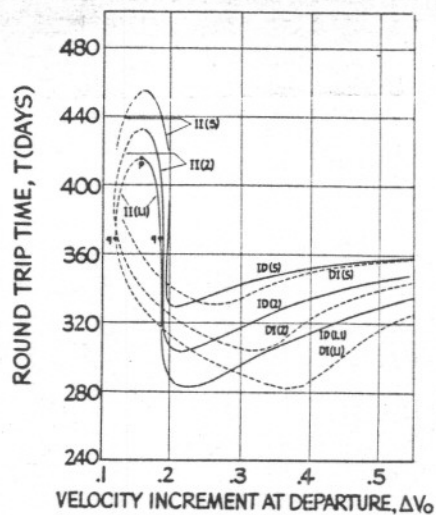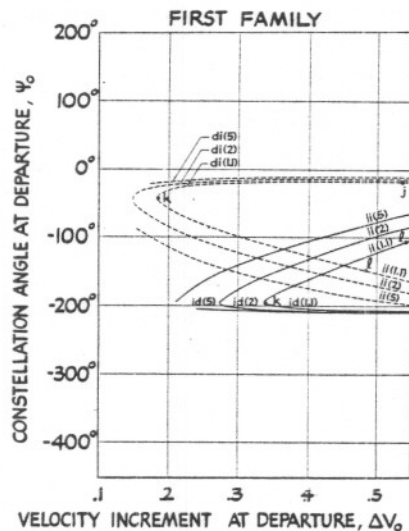V. R. a) First Family Swing-in b) First Family Swing-out

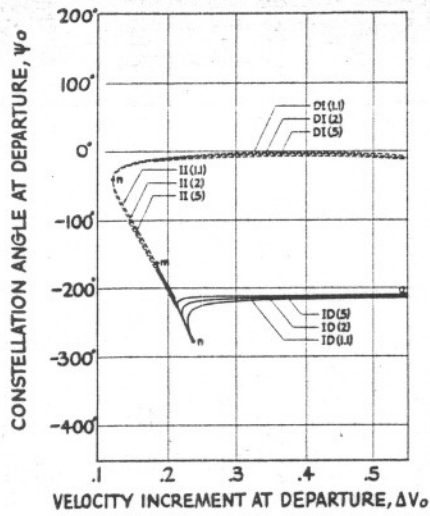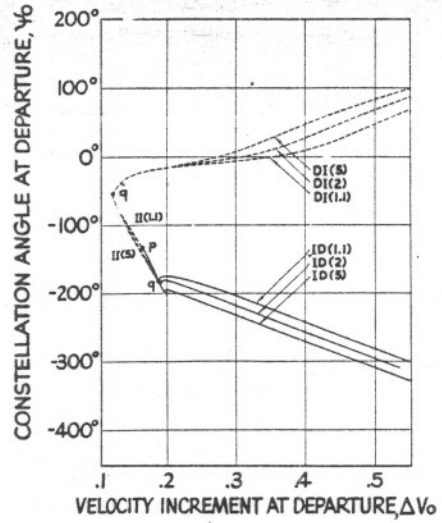Fig. 10   Second Family Swing-in   Second Family Swing-out
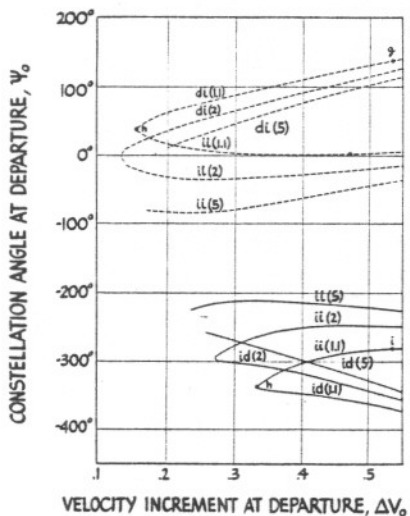
(a)   (b)

Fig. 11 Departure Constellation Angle vs. Velocity Increment (normalized with the heliocentric velocity of Earth) for Swing-Around-Venus Trajectories. Parking Orbit 1.1 E.R. Closest Approach 1.1, 2, 5 V.R. a) First Family Swing-in b) First Family Swing-out
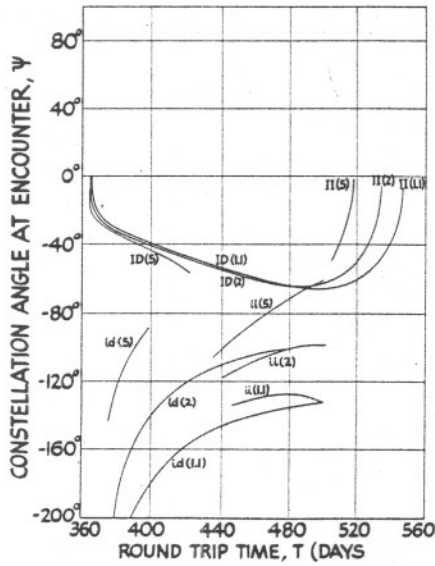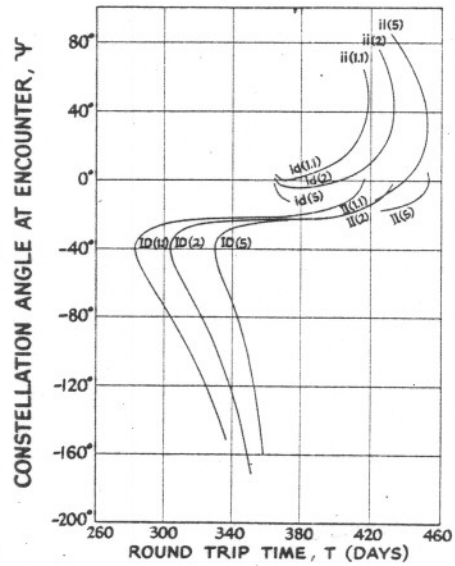
(c)

Fig. 11 Second Family Swing-in

(d)

Second Family Swing-out

(a)

(b)

Fig. 12 Encounter Constellation Angle vs. Total Trip Time for Swing-
Around-Venus Trajectories. Parking Orbit 1.1 E.R. Closest
Approach 1.1, 2, 5 V.R. a) Swing-in b) Swing-out

Characteristics of Swing-Around Trajectories

Figures 7 through 12 illustrate the characteristics of swing-around Mars and swing-around Venus trajectories. These charts present four items of interest: total trip time, constellation angles at departure and encounter, and velocity increment required to depart from a geocentric circular parking orbit with radius equal to 1.1 Earth radii.

Figure 7a and 7b illustrate two classes of round-trip Martian trajectories; the lower curves indicating trajectories of about one-year duration, the upper curves trajectories of about 1 1/2 to 1-3/4 years. A swing-in trajectory of somewhat less than 1-1/2 year duration exhibits the minimum velocity requirement ($\sim$ 4 mi/sec). Figures 8a and 8b illustrate the constellation angles at departure. It is interesting to note that these angles are grouped into three different ranges, one extending between 90° and 180°, and two narrow ranges grouped around 0° and 180°. Therefore, departure is possible during one quarter of the synodic year when Mars leads Earth and during a short period of time near inferior conjunction of the planets. The lower velocity requirements are associated with Martian lead angles of 106° to 126°. Figures 9a and 9b present constellation angles at planetary encounter vs. round-trip time. Such information is important in determining communication distance between Earth and vehicle at planetary encounter. Comparison of Figs. 7a and 9a illustrates the fortunate happenstance of minimum communication distance (zero constellation angle) occurring with minimum velocity requirements and shortest total trip for the longer than one-year family. If one knows constellation angles at both launch and encounter, he can, by means of a very simple calculation, determine the transfer times for each leg. Each transfer time is merely equal to the quotient of the change of constellation angle and the difference of planetary mean motions.

$$t = \frac{\psi - \psi_0}{n - n_E}$$

615

For Venusian orbits, the second family of swing-out trajectories, Fig. 10d exhibits the most favorable combinations of trip time and velocity requirements. The duration of these trips is between 3/4 and 1-1/4 years with velocity requirements at departure as low as 2.2 mi/sec. The range of constellation angles associated with these conditions lies between -50° and -200°. Thus, favorable departure is possible during almost half of the synodic year. But as can be seen from Figs. 11a through 11d, trips can be undertaken at any time if velocity increments up to 10 mi/sec are available. The comments regarding Figs. 7a and 9a for Martian trajectories apply also to Figs. 12a and 12b for Venusian voyages.

Initial Conditions for Swing-Around Trajectories

This section concerns itself with the initial conditions required as input for an n body precision orbit computation routine. Both initial and arrival conditions are needed, as the latter lead directly (by reversing the sign of the velocity vector) to initial conditions for clockwise trajectories. It was decided to present conditions at closest planetary approach rather than in terms of Earth departure and arrival conditions. This reduces the required amount of data by half, since the arrival and departure conditions at closest planetary approach are identical and both legs of the trajectory may be obtained by running forward and backward in time. Even more important, any errors resultant from the numerical calculations are now split into two segments rather than accumulating for the the entire duration of the mission. Therefore, the following data are presented: constellation angle at planetary encounter, location of closest approach (vertex of the planetocentric hyperbola) and velocity at this point expressed in units of planetocentric Kepler number. As explained above, these data can serve as initial conditions for both legs of the mission for precision calculation routines by running time in both positive and negative directions. If the resultant trajectory cuts the Earth's orbit either ahead or behind the Earth on both ends, the location of
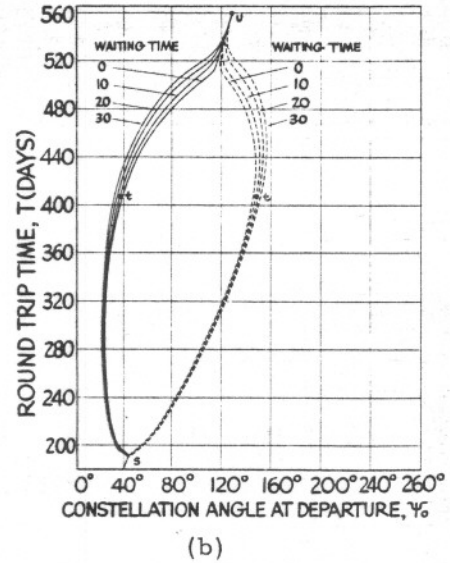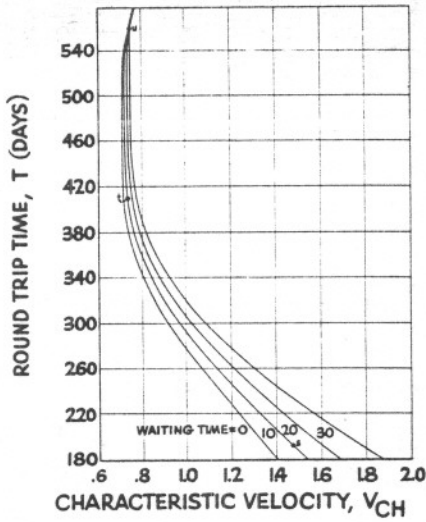
Fig.
city
74
c.
dies
ing
a
ents
and
usian

input
ar-
g the
tories.
rather
ces
con-
the
e.
cu-
r the
re
losest
is
ained
e
osi-
rth's

(a)

(b)

Fig. 13 Optimum Martian Round-Trip Trajectories. Parking Orbits =
1.1 E.R. and 1.1 M.R. a) Round-Trip Time vs. Characteristic
Velocity (normalized with the heliocentric velocity of Earth)
b) Round-Trip Time vs. Departure Constellation Angle

(a)

(b)

Fig. 14 Optimum Venusian Round-Trip Trajectories. Parking Orbits =
1.1 E.R. and 1.1 V.R. a) Round Trip Time vs. Characteristic
Velocity (normalized with the heliocentric velocity of Earth)
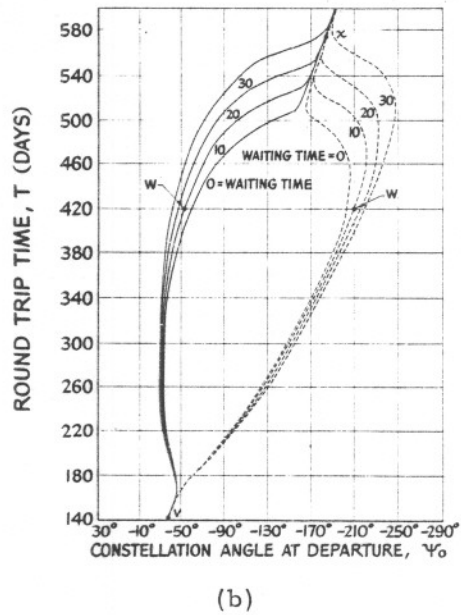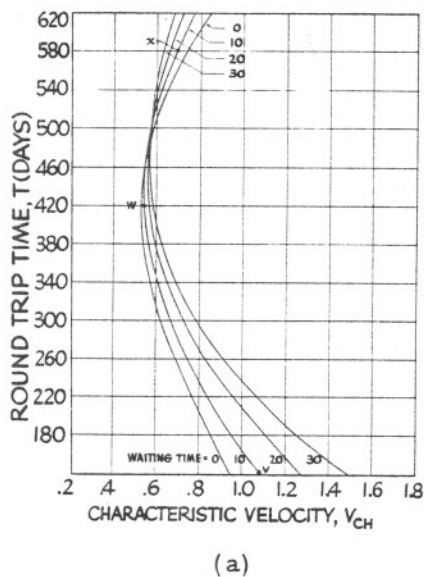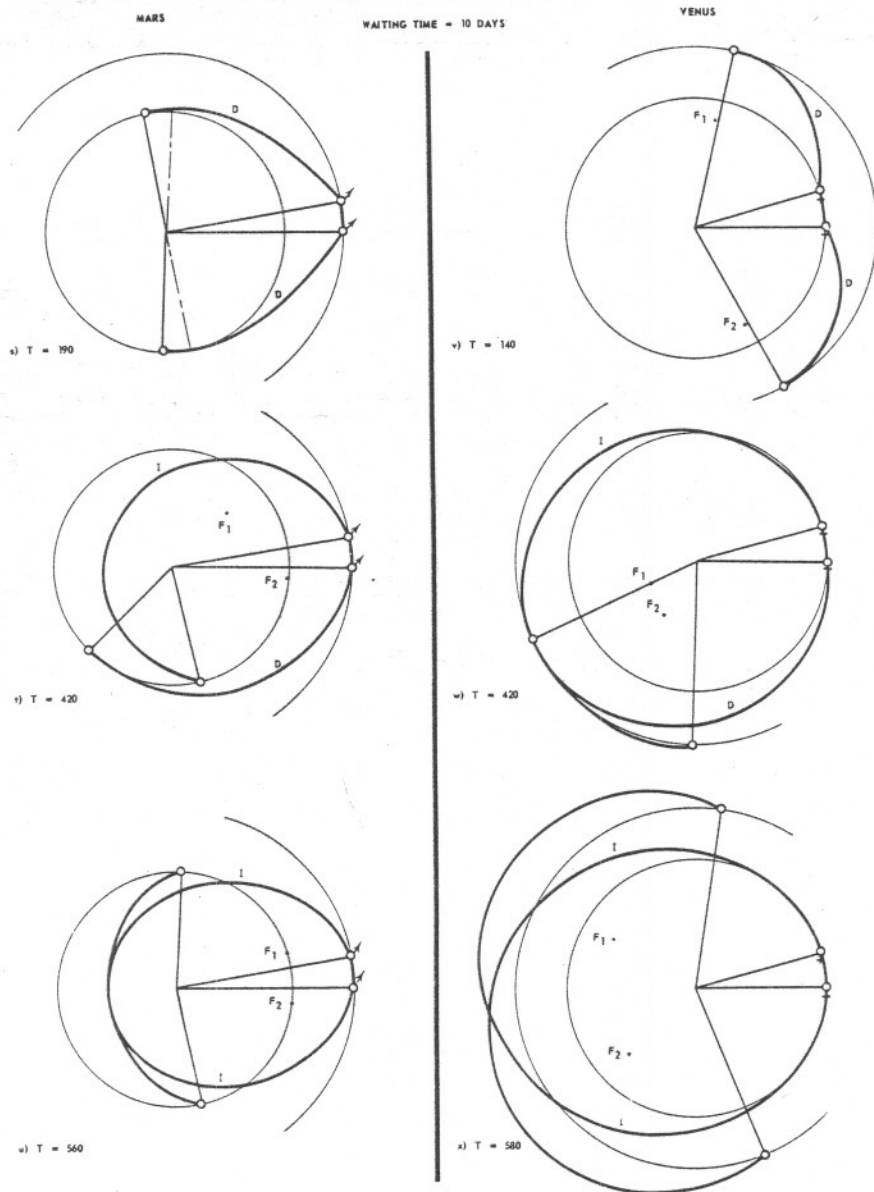b) Round-Trip Time vs. Departure Constellation Angle

617

MARS   WAITING TIME = 10 DAYS   VENUS

s) T = 190   v) T = 140

t) T = 420   w) T = 420

u) T = 560   x) T = 580

Fig 15   Orbiting Round-Trip Trajectories

closest approach should be adjusted. If, on the other hand, the trajectory branches "straddle" Earth, the velocity magnitude should be modified to achieve impacts. *

Characteristics of Optimum Orbiting Round-Trip Trajectories

Figures 13a through 14b present the characteristics of Optimum Round-Trip trajectories to Mars and Venus, involving waiting times of 0, 10, 20 and 30 days. During this waiting period, the spacecraft travels on a planetary parking orbit of 1. 1 planetary radius. The orbital characteristics illustrated in these figures are: round-trip time, constellation angle at departure, and characteristic velocity (sun of the four impulses). Minimum characteristic velocities are obtained for zero waiting time for trip times of approximately 500 days for Martian and 420 days for Venusian trajectories. These velocity requirements are 13. 1 mi/sec and 10. 2 mi/sec for Martian and Venusian voyages, respectively. Waiting time increases the characteristic velocity requirements for Martian trajectories but does not affect the trip time associated with minimum characteristic velocity. For Venusian voyages, waiting increases the round-trip time associated with minimum characteristic velocity. However, the velocity requirement increases less severely than for Martian trajectories.

Figures 13b and 14b yield the interesting result that, for short and long round-trip times, the optimum orbiting round-trip trajectories consist of symmetrical segments resulting from the fact that the clockwise and counterclockwise segments are identical. This symmetry does not hold for trip times of intermediate duration. The constellation angle range is restricted to allow for departure during about 2/5ths of the synodic year for Martian and over 1/2 of the synodic year for Venusian trajectories. Figure 15 shows round-trip trajectories for Mars and Venus.

---

* For accurate charts, apply to Northrop Space Laboratories and cite NSL62-83.

Initial Conditions for Optimum Orbiting Round-Trip Trajectories

This section concerns itself with the initial conditions at departure from a 1.1 Earth radii parking orbit. The characteristics shown are: constellation angle, velocity increment, and departure point location. Full line curves represent initial conditions for counterclockwise trajectories, dashed curves for clockwise trajectories. *

Constants

The following constants were used in the trajectory calculations:

	Radius of Parking Orbit	Earth	Mars	Venus
R_P/R_E	----	1	1.52369	.72333
V_P/V_h	1.1	.25323	.14	.199
	2	----	.1039	.1476
	5	----	.0657	.0933
$1/n_E$		58.134778 days/radians		

Non-Coplanar Trajectories

In the body of this report the assumption was made that the trajectory of the vehicle lies in the plane of the planetary orbits which were, in turn, assumed to be coplanar. In Appendix B, the necessary modifications for adapting the initial conditions to the non-coplanar case will be discussed.

REFERENCES

1. G. S. Gedeon, "Lambertian Mechanics," Proc, XII Internat. Astr naut. Cong. Also, "Orbital Segment Machanics," Norair report ASG-TM-61-43R

2. K. A. Ehricke, C. M. Whitlock, R. L. Chapman, and C. H. Purdy, "Calculations on a Manned Nuclear Propelled Space Vehicle", ARS

*See earlier footnote

Preprint 532-57

3. R. H. Battin, "The Determination of Round-Trip Planetary Reconnaissance Trajectories." Aero/Space Sci, Sept. 1959

4. P. G. Johnson, and R. L. Smith, "Round-Trip Trajectories for Mars Observation," Advances in the Astronaut. Sci, Vol. 5, Plenum Press, 1960

5. W. E. Moeckel, "Interplanetary Trajectories with Excess Energy," Proc. IX Internat Astronaut Cong, Springer Verlag, 1959

6. J. F. Dugan, Jr., "Analysis of Trajectory Parameters for Probe and Round-Trip Missions to Mars," NASA TN D-281, 1960

7. M. Vertregt, "Interplanetary Orbits" J. Brit. Interplanetary Soc. Mar-Apr 1958

8. J. F. Dugan, Jr., and C. R. Simsic, "Analysis of Trajectory Parameters for Probe and Round-Trip Missions to Venus," NASA TN D-470, 1960

9. G. S. Gedeon, "A Minimal Set of Orbital Equations," Norair report ASG-TM-61-63

HYPERBOLIC ENCOUNTER
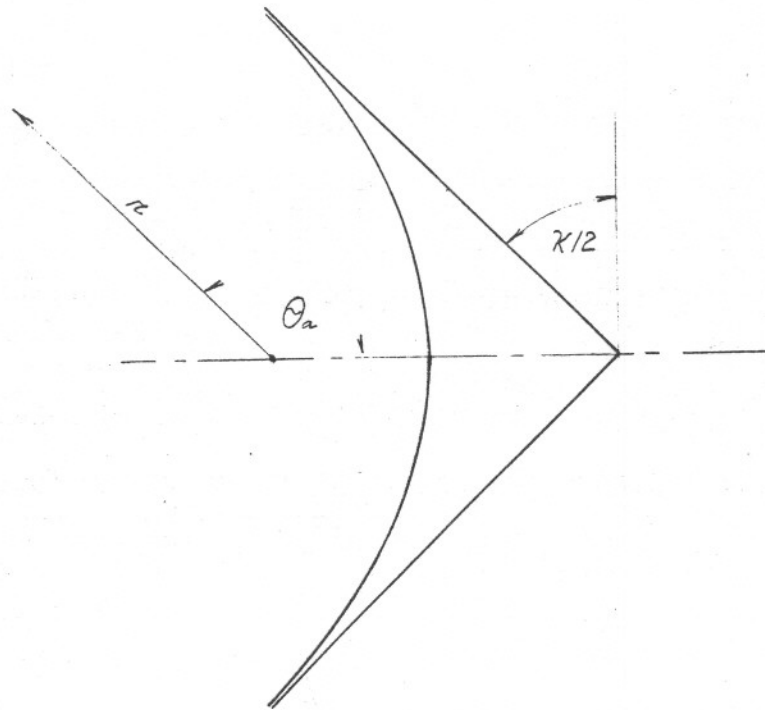
The true anomaly of the asymptote is found by equating the radius to infinity in the defining equation of a conic section

$$r = \frac{(1-e^2)\, a}{1 + e \cos \theta} \tag{1A}$$

yielding

$$\cos \theta_a = -\frac{1}{e} \tag{2A}$$

According to Ref. 9, the eccentricity is given by

$$e = \sqrt{1 - 4q(1-q)\cos^2\phi} \tag{3A}$$

where q is defined as $r/2a$ and called the modulus. At periplanet, the closest approach to the planet, the angle of elevation is zero and therefore

$$e = 1 - 2q_p \tag{4A}$$

In the same reference the relation between the modulus and Kepler number is given as

$$K = \sqrt{2(1-q)} \tag{5A}$$

Thus, the eccentricity expressed by the periplanet Kepler number becomes

$$e = K_p^2 - 1 \tag{6A}$$

and, finally, the true anomaly of the asymptote is

$$\cos\theta_a = -\frac{1}{K^2 - 1} \tag{7A}$$

From the sketch, it can be seen that half of the deflection angle K is

$$K/2 = \theta_a - 90° \tag{8A}$$

Therefore,

$$\sin K/2 = -\cos\theta_0 = \frac{1}{K_p^2 - 1} \qquad 0 \le \frac{K}{2} \le \frac{\pi}{2}. \tag{9A}$$

Now the vertex velocity is the square root of the sum of the square of the escape velocity and the square of the hyperbolic excess velocity. If unitless velocity expressions are used, the heliocentric hyperbolic excess Kepler number $K^{h.e.}$ must be converted into a planetocentric hyperbolic excess Kepler number. This is accomplished by applying the (V_p/V_h) conversion factor

$$K_p^2 = 2 + \left[\frac{K^{h.e.}}{V_p/V_h}\right]^2 \tag{10A}$$

Combining Eqs. (9A) and (10A) yields

$$\csc K/2 = \left[\frac{K^{h.e.}}{v_p/V_h}\right]^2 + 1 \qquad (11A)$$

APPENDIX B

NON-COPLANAR ENCOUNTER

This appendix is concerned with obtaining initial conditions for non-planar spatial trajectories made necessary by the fact that the planetary orbits are not coplanar. Planetocentric hyperbolas which are "skewed" with respect to the planetary orbit plane will yield such type of trajectories. In order to utilize initial conditions obtained in the coplanar analysis, the following assumptions must be made:

1) The vertex of the planetocentric hyperbolas should be on the sun-planet line,

2) The earlier obtained $(K, \emptyset, \sigma)_{1, 2}$ sets are to be maintained intact. Utilizing above assumptions, one finds that the deflection angle $\acute{K}'$ will be larger than the K associated with the coplanar case if $(K, \emptyset, \sigma)_1$, and $(K, \emptyset, \sigma)_2$ are to be preserved. Simple vector algebra yields the relationship between $\acute{K}'$ and $\acute{K}$ as

$$\tan \acute{K}'/2 = \frac{\tan K/2}{\cos i} \tag{1B}$$

Now Eq (9A) can be written as

$$\tan K/2 = \frac{1}{K_p\sqrt{K_p^2 - 2}} \tag{2B}$$

Letting K'_p designate the planetocentric Kepler number at closest approach which produces the deflection angle K', Eq (2B) can be rewritten for prime values and then combined with Eq (1B) to yield

$$K'_p\sqrt{K_p^{'2} - 2} = K_p\sqrt{K_p^2 - 2} \quad \cos i \tag{3B}$$

or

$$K_p' = \left[1 + \sqrt{1 + K_p^2 (K_p^2 - 2) \cos^2 i} \right]^{1/2} \quad (4B)$$

Also, by combining Eqs (10A) and (4B) one obtains

$$(V_p/V_h) = \frac{K^{h.\,e.}}{\sqrt{K_p'^2 - 2}} \quad (5B)$$

Therefore, the results of the coplanar investigations remain valid if K_p and the radius of closest approach are modified according to the last two equations (before inserting those as initial conditions into a precision trajectory calculation routine).

The plane changes i_1 and i_2 (in heliocentric space) with respect to the planetary orbit plane are obtained from the following relations:

$$K_1 \sin \phi_1 \sin i_1' = K^{h.\,e.} \cos K'/2 \, \sin i = K_2 \sin \phi_2 \sin i_2 \quad (6B)$$

From this last equation, it is evident that in general $i_1 + i_2$, and hence a net plane change was affected by the gravitational field of the planet without exterior propulsion.

eighth
annual
meeting

Volume 11
ADVANCES IN THE ASTRONAUTICAL SCIENCES

Edited by Horace Jacobs

1963